Proc. Estonian Acad. Sci. Phys. Math., 2001, **50**, 4, 227–246

ELECTRON PARAMAGNETIC RESONANCE SPECTRA OF HUMAN TOOTH ENAMEL WITH PREFERENTIALLY ORIENTED NANOCRYSTALS

Georg LIIDJA

National Institute of Chemical Physics and Biophysics, Akadeemia tee 23, 12618 Tallinn, Estonia; gli@kbfi.ee

Received 15 June 2001, in revised form 21 August 2001

Abstract. Electron paramagnetic resonance spectra of a selected γ-irradiated human tooth enamel fragment expressed anisotropy that increased considerably after thermal annealing. By repeated irradiation, the spectrum of the fragment approached the disoriented (powder type) spectrum, but repeated thermal treating restored the anisotropy. The anisotropy is characteristic of an ensemble of hydroxyapatite nanocrystals, predominantly oriented with the hexagonal axis perpendicular to the outer surface of the tooth. A Monte Carlo spectral simulation, corresponding to the bulk arrangement of paramagnetic CO_2^- radicals possessing the C_{2v} symmetry and normal distribution of *y*-axes (parallel to the O–O direction) in a space angle of 27° (±5°) around the surface normal, gives a satisfactory agreement with the experimental spectra, whereas the agreement for alternative models with specific surface arrangement of the radicals is worse.

Key words: electron paramagnetic resonance, irradiated tooth enamel, CO_2^- radicals, spectral anisotropy, Monte Carlo simulation.

1. INTRODUCTION

Paramagnetic defects are formed in tooth enamel after ionizing irradiation. This quality is used in electron paramagnetic resonance (EPR) dosimetry and dating (e.g. [1]). Paramagnetic signal, which is proportional to the acquired dose, is represented as a number of created stable carbonate radicals, the majority of radicals being CO_2^- molecule-ions [2]. The location of radiation induced carbonate radicals in tooth enamel and other calcified tissues is a question of issue (see, e.g., [3], Ch. 4.7, and [4,5]). Here we make an attempt to distinguish

between various possibilities by analysing details of EPR spectra of oriented pieces of human tooth enamel.

Electron microscopic investigations [6] have revealed that hydroxyapatite nanocrystals, the main inorganic constituent of enamel, are enmeshed in the organic matrix consisting of prismatic elements that lie preferentially parallel to each other, with the long axis perpendicular to the enamel surface. Hexagonal hydroxyapatite crystals, with the average size of 600–870 Å [7] can be as long as 10 000 Å. Inside prisms they are parallel or at angles of 20–40° to the long axes of prisms and lie obliquely or even perpendicularly in the areas between prisms. The organic part (eukeratin, composed of collagenous material, hydroxyproline, glycoprotein, and citric acid) is only 0.4–0.9% of the enamel [8]. The organic part and water molecules on the crystal surfaces mostly escape enamel during thermal treatment above 400 °C [5,9].

There are three kinds of precursors of CO_2^- radicals in biological apatite (carbonated hydroxyapatite $Ca_{10-x+y}(PO_4)_{6-x}(CO_3)_x(OH)_{2-x+2y}$ [10]): (i) a carbonate group $(CO_3)^{2-}$ can replace either $(OH)^-$, which is called A-type replacement, or (ii) $(PO_4)^{3-}$, which is called B-type replacement, and (iii) a CO_2 molecule can absorb on the organic or hydration layer on the crystal surface. Relevance of the atmospheric carbon dioxide is confirmed in experiments where hyperfine structure is clearly resolved in the spectra of irradiated synthetic apatite powders which have been exposed to the ^{13}C enriched CO_2 atmosphere [11–13]. The values of the *g*-tensor components in orthorhombic CO_2^- depend little on where the molecules are situated, in the bulk or on the surface [14]. In some samples an isotropic line of the same radical is seen, which is attributed to CO_2^- molecules tumbling in occluded water [15]. Their contribution to the EPR absorption is much less than that of orthorhombic species.

Small pieces of human [5,16–18] and also fossil (e.g. shark and mastodon [19]) dental enamel reveal orientation effects in their spectra when rotated in the magnetic field. The angular variation of enamel spectra corresponds only roughly to what is expected in the case of monocrystals. For instance, the minimum at the high field end of the first derivative spectrum $(g_y = 1.9975)$ changes its intensity and not the position for some enamel fragments rotated in the magnetic field. Further, spectra of various paramagnetic species (CO_2^- in different positions, CO_3^{3-}) overlap each other, which notably complicates decomposition of spectra [5,20].

Below we describe some methods of spectral decomposition with the emphasis on distinguishing CO_2^- molecules of orthorhombic (or axial) symmetry in the bulk or on the surface layer of hydroxyapatite nanocrystals and apply these for powder specimens and a piece of irradiated human enamel containing relatively well-aligned crystallites. Reversible changes of spectral anisotropy during thermal treatment and reiterated irradiation of the sample are analysed.

2. MATERIALS AND METHODS

Powder-like spectra of tooth enamel were measured on ground and sieved (0.1–0.25 mm grains) samples from a collection of wisdom teeth supplied by the Kiev Student Clinic [21]. The pool was great enough to represent average teeth.

The powdered sample *Wies 100 kGy* was irradiated in December 2000 at the GSF facilities (Neuherberg, FRG) with a ^{60}Co γ-ray dose of 100 kGy.

The powdered sample *3 kGy + T* was irradiated in January 1999 at the 5 kCi ^{60}Co facility of the Institute of Experimental Biology (Harku, Estonia), heated for 40 min at 195 °C, and held at ambient conditions until measurements.

The sample *Glie* was a 16 mg piece cut from the proximal surface of a canine. Due to the constricted area this surface was quite flat (as compared to concave lingual and convex buccal sides). During the first measurements (in 1993) we detected anisotropy of the EPR spectrum developing during the heating of the fragment irradiated with a γ-dose of 500 Gy.

Electron paramagnetic resonance spectra were measured on the ERS 230 spectrometer and registered either on the paper or transmitted to the Toshiba Satellite 2180 CDT portable personal computer through the analogue-digital virtual instrument pod system (Thurlby Thandar Instruments VIPS10). For spectral corrections the lines of additively coloured CaO ($g = 2.0001$) and MgO:Cr ($g = 1.980$) were used. Experimental spectra are presented with the magnetic field values (in Gauss) as the argument. Ordinate values are in millimetres for paper diagrams (referred to as arbitrary units) and in Volts for VIPS10 (1 Volt equals approximately 180 mm).

3. SPECTRAL DECOMPOSITION

The recorded spectra were compared with theoretical spectra. In the literature [22,23], formal decompositions of enamel spectra into 2–5 Gaussian or Lorentzian bands are used, which are very rough approximations for molecules of axial or orthorhombic symmetry. A more rigorous lineshape calculation by Callens et al. [24] is also based on approximations but is suitable for a least squares fitting of experimental data. To our knowledge, the original treatise on orthorhombic powder spectra by Kneubühl [25] has not been used in papers dealing with tooth enamel. Below we shall give a brief summary of Kneubühl's formulae for randomly oriented $S = \frac{1}{2}$ systems (neglecting hyperfine splitting and lifetime broadening).

If the principal *g*-tensor values are $g_1 < g_2 < g_3$ (and the corresponding magnetic field values for lines in ideal monocrystals $H_1 > H_2 > H_3$), then the normalized shape function $S(H)$ for running magnetic field values $H_3 < H < H_2$ is

$$S(H) = \frac{2H_1H_2H_3c(k)}{\pi H^2(H_1^2 - H^2)^{1/2}(H_2^2 - H_3^2)^{1/2}}, \tag{1}$$

with

$$k^2 = \frac{(H_1^2 - H_2^2)(H^2 - H_3^2)}{(H_1^2 - H^2)(H_2^2 - H_3^2)}, \tag{2}$$

and for $H_2 < H < H_1$

$$S(H) = \frac{2H_1H_2H_3c(1/k)}{\pi H^2(H_1^2 - H_2^2)^{1/2}(H^2 - H_3^2)^{1/2}}. \tag{3}$$

Here $c(k)$ is the complete elliptic integral of the first kind

$$c(k) = \int_0^{\pi/2} \frac{d\alpha}{\sqrt{1 - k^2 \sin^2 \alpha}}, \tag{4}$$

with values $c(0) = \pi/2$ at the endpoints $(H = H_1, H = H_3)$ of the spectrum. At $H = H_2$ the complete elliptic integral diverges. An appropriate value of $c(H_2)$ can be found from the normalization condition of the shape function $\sum S(H)\delta H = 1$, where δH is the magnetic field increment used for approximation.

The shape function has to be convoluted with the appropriate Gauss or Lorentz function for comparison with the experimental (integrated) spectrum.

Another possibility we used was Monte Carlo simulation, with the application of the random number generator built into the program ORIGIN 6.1. Here we got the normalized shape function by choosing the three values of the *g*-tensor components from the powder spectra and appropriate Eulerian angle values for the molecular axes β and γ in the magnetic field reference frame (Fig. 1). Then the spectral position of each of the (say) 100 000 radical lines is determined by

$$g^2 = g_3^2 \sin^2 \beta \sin^2 \gamma + g_2^2 \sin^2 \beta \cos^2 \gamma + g_1^2 \cos^2 \beta, \tag{5}$$

where γ is the angle by which the molecule has to be rotated around its *z*-axis (corresponding to g_1) and β is the angle of the second rotation around the new *y*-axis until the new *z*-axis coincides with the magnetic field direction z'. The shape function is the histogram. As previously, the shape function has to be convoluted with the appropriate Gauss or Lorentz function.

The above two methods are compared in Fig. 2. The shape function's maximum for Monte Carlo simulation is higher than for Kneubühl's theory, because the divergence point $H = H_2$ is underestimated (marked by an arrow) in this particular case. However, absorption curves obtained with the two methods are not much different.

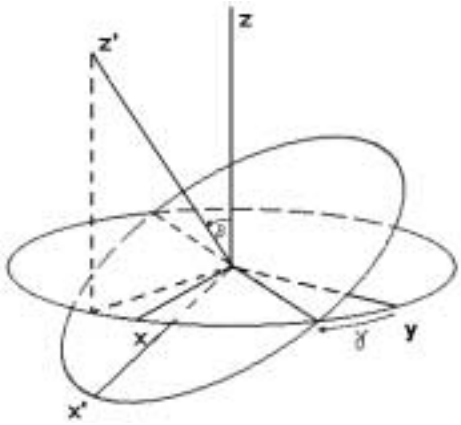

Fig. 1. Eulerian angles. Molecular reference axes are *x*, *y*, *z*, magnetic field reference system is primed ($H \| z'$).

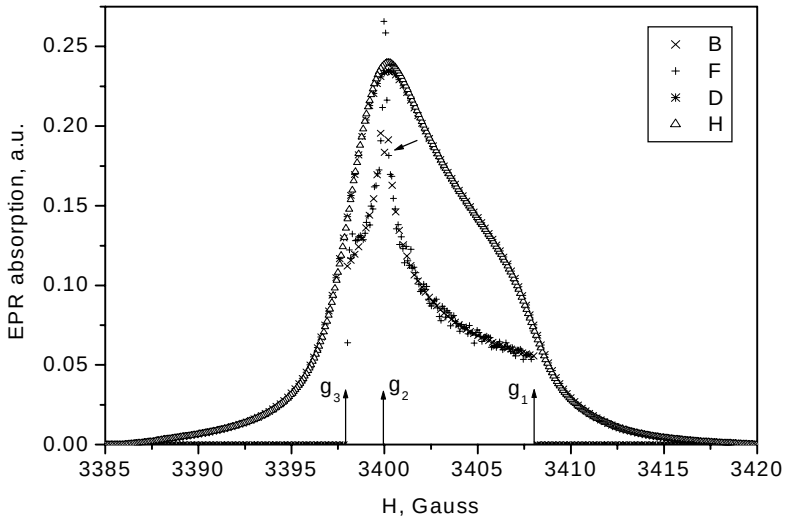

Fig. 2. Shape functions (B, F) and respective convolutions (D, H) for EPR spectra of paramagnetic molecules with orthorhombic symmetry. B was obtained using Kneubühl's formulae (1–4) with H_1 = 3408 G, H_2 = 3400 G, H_3 = 3398 G; δH = 0.2 G. 100 000 points Monte Carlo simulation according to (5) with gH = 6807.48, bin width δg = 0.00005 resulted in curve F. In both cases convolution was made with the Lorentz function $L = 2.25/(2.25 + (H - H_0)^2)$.

Below we shall adopt the molecular reference system with the *x*-axis perpendicular to the plane of the (nonlinear) CO_2 molecule, the *y*-axis parallel to the line connecting oxygen nuclei, and the *z*-axis coincident with the molecular C_2-axis. The principal values of the *g*-tensor for the CO_2^- radical are $g_x > g_z > g_y$ [26].

For the case of axial symmetry we adopt the following notations: $g(parallel) = g_y$ and $g(perpendicular) = g_x$. The shape function is (Sands, cited after Kneubühl [25])

$$S_{\mathrm{ax}}(H) = H_x^2 H_y (H_x^2 - H_y^2)^{-1/2} H^{-1/2} (H_x^2 - H^2)^{-1/2}. \tag{1a}$$

Alternatively, Monte Carlo simulation is easily performed using

$$g^2 = g_x^2 \sin^2\beta + g_y^2 \cos^2\beta. \tag{5a}$$

4. SPECTRA

4.1. Grained enamel

Figure 3 shows the X-band (9.2 GHz) spectrum of grained tooth enamel (sample *Wies 100 kGy*). The spectrum was approximated as a sum of the orthorhombic contour of CO_2^- comprising 90% of the total area under the absorption curve and two additional Gaussian curves in the low field part of the spectrum. The former is satisfactorily approximated with Monte Carlo simulation using the *g*-tensor components $g_y = 1.9975$, $g_z = 2.00205$, $g_x = 2.0032$, and the Lorentz bandwidth $\Gamma = 1.5\,\mathrm{G}$.

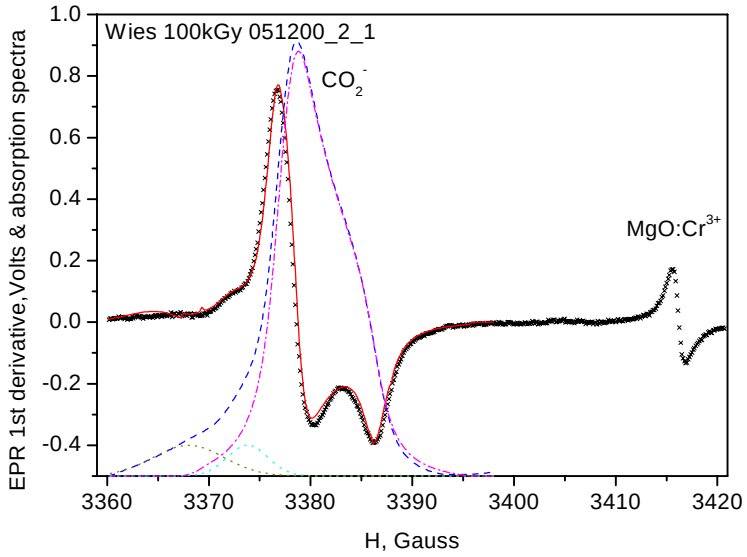

Fig. 3. The EPR spectrum of the 13.8 mg sample *Wies 100 kGy* is given with crosses. During the run the enamel sample in the cavity was replaced with the MgO:Cr sample containing 8×10^{13} Cr^{3+} ions (spin 3/2). The integrated spectrum of the enamel (dashed), approximated contours of orthorhombic CO_2^- (dash-dotted), and minor additions (dotted) are baseline-shifted for clarity. The solid line is the derivative of the approximated spectrum. Measurement conditions: 14 mW klystron power, 0.5 G 100 kHz modulation amplitude, 18 dB attenuation.

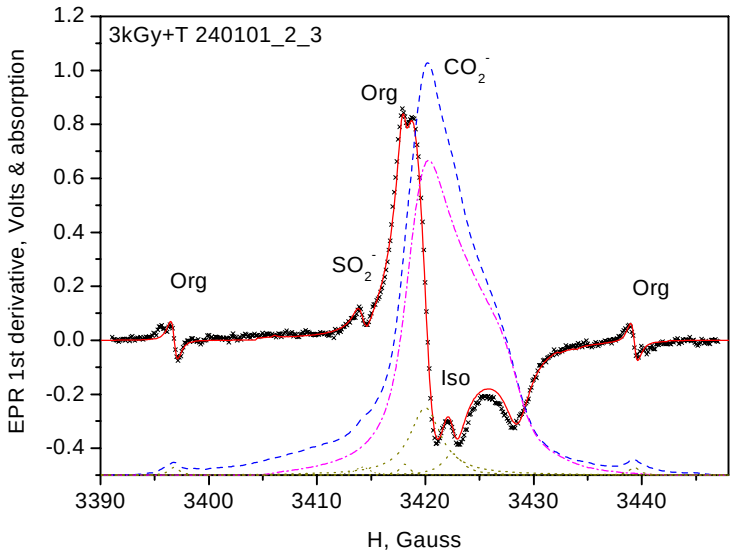

Fig. 4. The EPR spectrum of the 20 mg sample *3 kGy + T* (crosses) was measured in the same conditions as the preceding sample. The integrated spectrum (dashed), approximated contours of orthorhombic CO_2^- (dash-dotted), and minor additions (dotted) are baseline-shifted. The solid line is the derivative of the approximated spectrum.

A grained enamel sample (Fig. 4), irradiated and heated $(3\,kGy + T)$, was approximated with the orthorhombic contour using $g_y = 1.99745$, $g_z = 2.00195$, $g_x = 2.0033$, and the Lorentz bandwidth $\Gamma = 1.5$ G that covers 85% of the total area under the absorption spectrum. Other bands (approximated as Lorentzians) in the actual part of the spectrum which arise (or sharpen) with thermal treatment belong to the isotropic CO_2^- at $g_1 = 2.0009$, $\Gamma = 1.2$ G; to SO_2^- (supposedly) at $g_S = 2.0057$, $\Gamma = 0.8$ G; to the central line of the organic septet at $g_{ORG} = 2.00345$, $\Gamma = 0.6$ G; and to unidentified species (probably to other carbonate radicals) at $g_U = 2.00235$, $\Gamma = 1.7$ G.

The values of *g*-tensor components of carbonate derived radicals are not fixed strictly; they can vary from sample to sample (and from paper to paper) by about $\Delta g = 0.0004$ (see also [2,3,5]). The above spectra and parameters of grained samples are further used as a model for the sample with the anisotropic spectrum.

4.2. Oriented fragment

Spectra of the enamel fragment rotated around the axis, perpendicular to both the field (***H***) and the tooth surface normal (***C***) are presented in Fig. 5, depending on the angle α between ***H*** and ***C*** as parameter. The sample has been irradiated with ^{60}Co γ-rays (dose 6.7 kGy) and heated to 270 °C for making the anisotropy

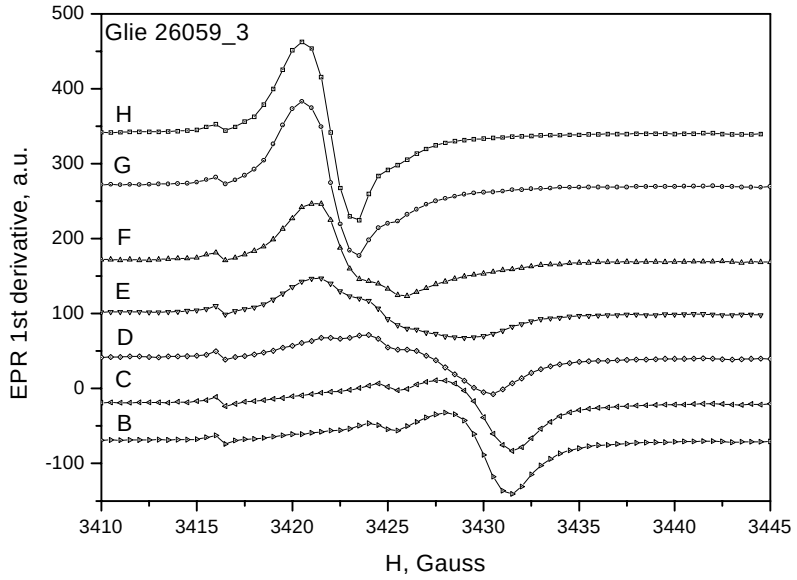

Fig. 5. The EPR spectra of the enamel sample *Glie*, γ-irradiated (accumulated dose 6.7 kGy) and heated in air for 30 min at 270 °C. Curves B–H correspond to the 15° rotations around the axis perpendicular to both the static field $\boldsymbol{H}$ and tooth surface normal $\boldsymbol{C}$ and are shifted vertically for clarity. Measurement conditions: 50 mW, 0.5 G, 24 dB.

maximal (see below). The main signal comes clearly from orthorhombic CO_2^-, showing a minimum at 3432 G in the derivative spectrum with $\boldsymbol{C}$ parallel to the field and a maximum at 3421 G from the spectrum with perpendicular orientation (in Fig. 5). In addition, the spectrum contains weaker bands at 3424 G (isotropic carbonate radicals) and 3416 G (SO_2^- radical). The so-called organic septet (central line at 3420 G) is almost quenched as a result of thermal treatment and saturation (microwave power was 50 mW).

Spectra for perpendicular and parallel orientation are shown separately in Fig. 6. They demonstrate the effect of repeated irradiation (with growing doses) and the influence of thermal treatment (after 6.7 kGy annealing for 20 min at 270 °C and after 107 kGy annealing for 12 min at temperatures indicated in Fig. 6). It should be emphasized that anisotropy builds up after annealing the sample and if repeatedly irradiated, the added part of the spectrum resembles that of the powder type. To characterize the above finding numerically, we make use of an anisotropy parameter defined as

$$A = \frac{B + C' - B' - C}{B + C' + B' + C}, \tag{6}$$

with the values $B, B', C,$ and C' defined in Fig. 7. In the monocrystal type spectrum of axial radicals for parallel orientation ($\boldsymbol{H} \| \boldsymbol{C}$) the line has intensity

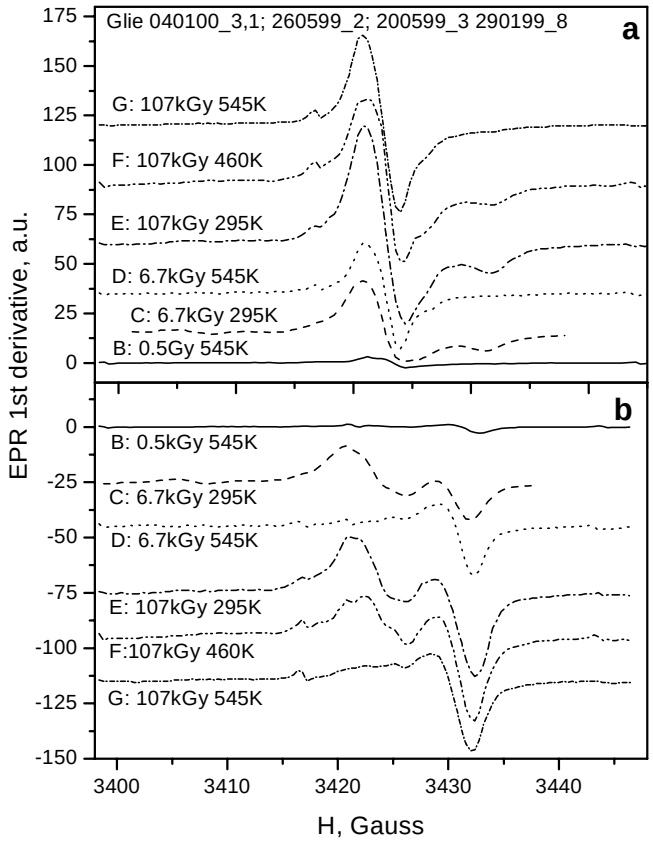

Fig. 6. The EPR spectra of the enamel sample *Glie* for $\boldsymbol{H} \perp \boldsymbol{C}$ (**a**) and $\boldsymbol{H} \parallel \boldsymbol{C}$ (**b**), measured after γ-irradiation with accumulated dose values and thermal annealing at absolute temperatures given at curves B–G. Baselines are shifted for clarity.

C, and $B = 0$; for perpendicular orientation the line has intensity B', and $C' = 0$; anisotropy has its maximal value $A = 1$. In the powder spectrum there is no angular dependence, $B = B'$, $C = C'$, and $A = 0$. The measurement depicted in Fig. 7 gives $A = 0.43$.

The anisotropy parameter is growing with the annealing at temperatures above 150 °C and exceeds 0.8 after annealing at 270 °C. The (normalized to the unannealed specimen) number of radicals N, measured as the (proportional) area under the integrated EPR spectrum, is also diminishing with annealing, but 55% of the initial number is preserved after heating at 270 °C. Both N (for N we take the sum of the areas measured at perpendicular and parallel orientation) and A are plotted in Fig. 8. In Fig. 9 the anisotropy factor is plotted logarithmically against T^{-1}, leading to the activation energy $E_{\mathrm{A}} = 0.12$ eV. This is three times less than the activation energy of the thermal destruction of radicals, obtained from the plot of the area under the integrated EPR spectrum,

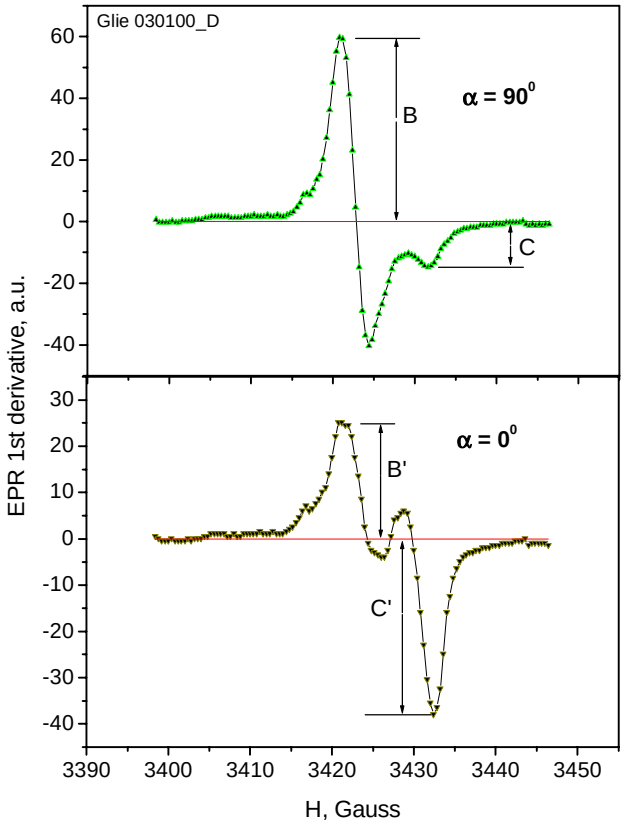

Fig. 7. Definition of the anisotropy parameter $A = (B + C' - B' - C)/(B + C' + B' + C)$ from the EPR spectra of the enamel fragment *Glie* (prehistory: 6.7 kGy >>270 °C >> 100 kGy >> RT). Measurement conditions: 1.6 mW, 0.5 G, 24 dB. Here $A = 0.43$.

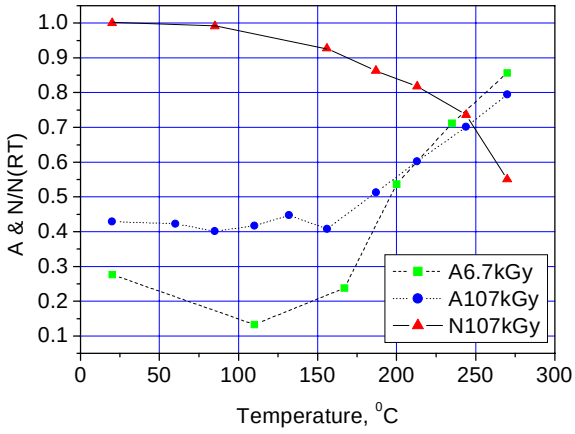

Fig. 8. Normalized number of the CO_2^- radicals (N) in the γ-irradiated enamel sample *Glie* and anisotropy factor (A) in dependence on the annealing temperature. Lines are drawn for the eyes guidance.

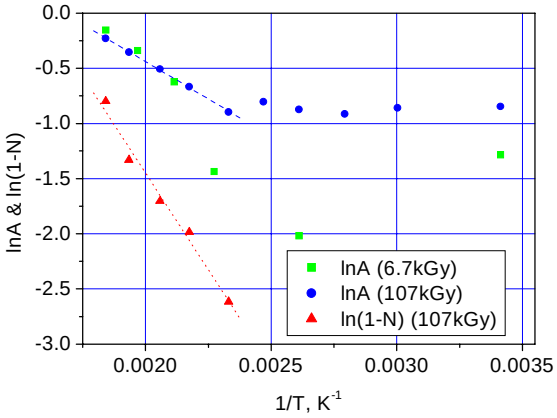

Fig. 9. Logarithmic plot of the data presented in Fig. 8 (points) and linear fits (lines).

E_D = 0.39 eV. However, if one plots the anisotropy which can be related to the radicals created by the last irradiation,

$$\Delta A = A(T) - < A(T < 440K) >, \tag{7}$$

where $< A(T < 440K) > = 0.42$ is the average value of A from the measurements at temperatures below 440 K, where it was nearly constant as it developed after the last irradiation, we get for activation energy a value of E_A = 0.4 eV. Earlier we have measured the activation energy of destruction of carbonate radicals from powder specimens at temperatures up to 700 K [16]. Although the overall dependence of the EPR signal amplitude did not correspond to the Arrhenius type logarithmic plot, the high temperature part of it could be approximated with a value E_D = 1.3 eV exceeding considerably the activation energy of anisotropy development (in [16] we overestimated E_A = 0.8 eV, using too few experimental data).

4.3. Surface position models

For the purpose of fitting the spectra with theoretical models we choose three spectra of the oriented fragment measured at α values of 0°, 45°, and 90°. They are presented in Fig. 10.

To confront bulk and surface positions, we use a simple model with axial molecules, $g_y < g_z = g_x$, that is qualitatively representing also orthorhombic molecules if $g_x - g_z << g_z - g_y$ (in the case of CO_2^- approximately $g_z - g_y = 4(g_x - g_z)$). Nanocrystals are described as having the shape of long cylinders (with top and bottom surfaces ignored). Paramagnetic molecules are oriented according to the symmetry of the cylinder.

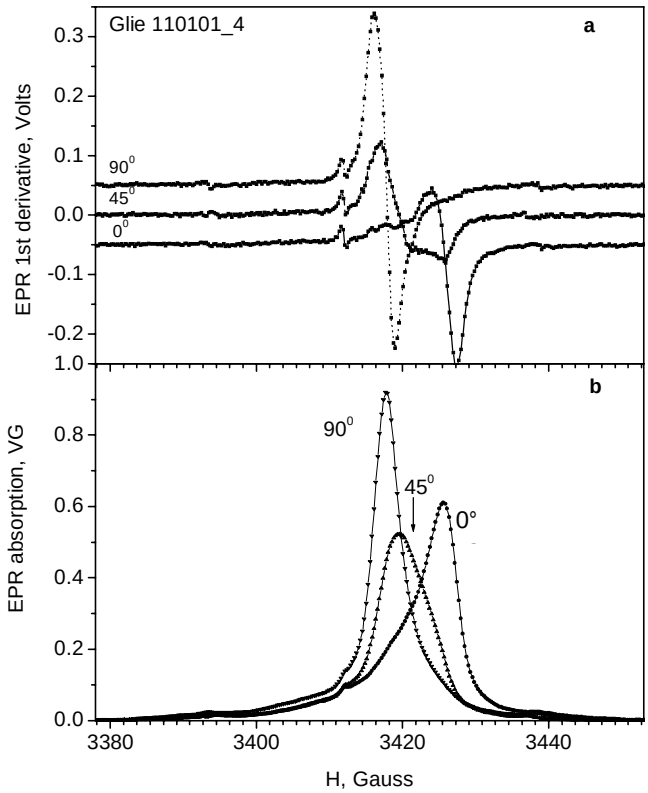

Fig. 10. (a) EPR spectra (marked with the orientation angle (α) values of 90°, 45°, and 0°) and (b) integrated spectra of the enamel fragment *Glie*, irradiated (107 kGy) and annealed (270 °C).

Figure 11 shows three of the four possible cases of orientation. Here we use the following notations: $\boldsymbol{K}$ is a vector directed along the cylindrical axis; $\boldsymbol{H}$ is a

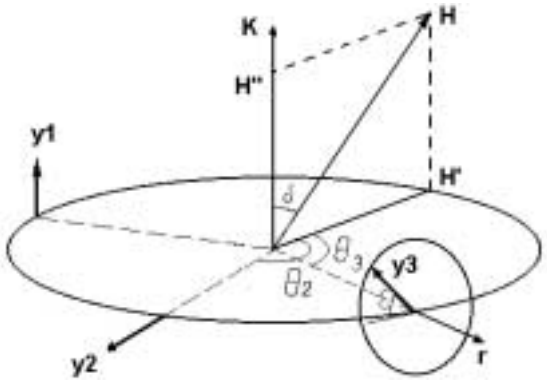

Fig. 11. Three cases for the axial molecule (axis *y*) situated on the surface of the cylinder with its axis $\boldsymbol{K}$ at the angle δ in respect of the field $\boldsymbol{H}$. θ is the angle of rotation around $\boldsymbol{K}$ and ε is the angle of rotation around the radial axis $\boldsymbol{r}$.

vector along the static magnetic field; y is the molecular axis; $\boldsymbol{H}'$ is the projection of the field in the plane perpendicular to $\boldsymbol{K}$; δ is the angle between $\boldsymbol{K}$ and $\boldsymbol{H}$, therefore $H' = H\sin\delta$; θ is the rotation angle around the axis of the cylinder; and ε is the rotation angle around the radial vector $\boldsymbol{r}$ that points to the molecule on the surface of the cylinder.

As before, α is for the *sample* orientation, β is the angle between the molecular axis and field, and $\alpha = \delta$ if the sample consists of strictly parallel nanocrystals.

We shall analyse four different cases for the shape function.

Case 1

$\boldsymbol{y} \| \boldsymbol{K} (\beta = \delta)$: molecules are arranged with their axes parallel to the cylinder. The spectrum consists of a line the spectral position of which is determined by the usual expression

$$g^2 = g_x^2 \sin^2\delta + g_y^2 \cos^2\delta, \tag{8}$$

where the density of states is infinite. This spectrum is isomorphic to the spectrum of similarly oriented bulk molecules.

Case 2

$\boldsymbol{y} \perp \boldsymbol{K}$: molecules are perpendicular to the surface of the cylinder. The shape is determined by

$$g^2 = g_x^2 - (g_x^2 - g_y^2)\cos^2\theta \sin^2\delta, \quad 0 < \theta < \pi/2. \tag{9}$$

The shape function is a band of width proportional to $\cos^2\delta$, the density of states is infinite in both margins. The spectrum is isomorphic to the spectrum of bulk molecules if they have their axes in a plane perpendicular to $\boldsymbol{K}$ and randomly oriented with respect to θ.

Case 3

$\boldsymbol{y} \perp \boldsymbol{r}$: molecules are on the surface with their axes lying in the tangential plane, randomly oriented with respect to the angle ε. The shape function reduces to

$$g^2 = g_x^2 - (g_x^2 - g_y^2)(\sin\varepsilon\cos\delta + \cos\varepsilon\sin\delta\cos\theta)^2, \; 0 < \varepsilon < \pi/2, \; 0 < \theta < \pi/2. \tag{10}$$

This case has no bulk analogue and is therefore discriminating.

Case 4

The axis y is randomly oriented over 4π. Here the shape function is the same as in the bulk arrangement and the spectrum is of the powder type. The shape function contains a factor $\sin\beta$ accounting for the integration over the space

angle (in cases 1–3 integration has to be performed over a circle around the cylinder with a uniform density of states).

Figure 12 represents shape functions, Lorentzian convolutions, and their derivatives for cases 1, 2, and 3 at angles $\alpha = \delta$ equal to 0°, 45°, and 90°. For

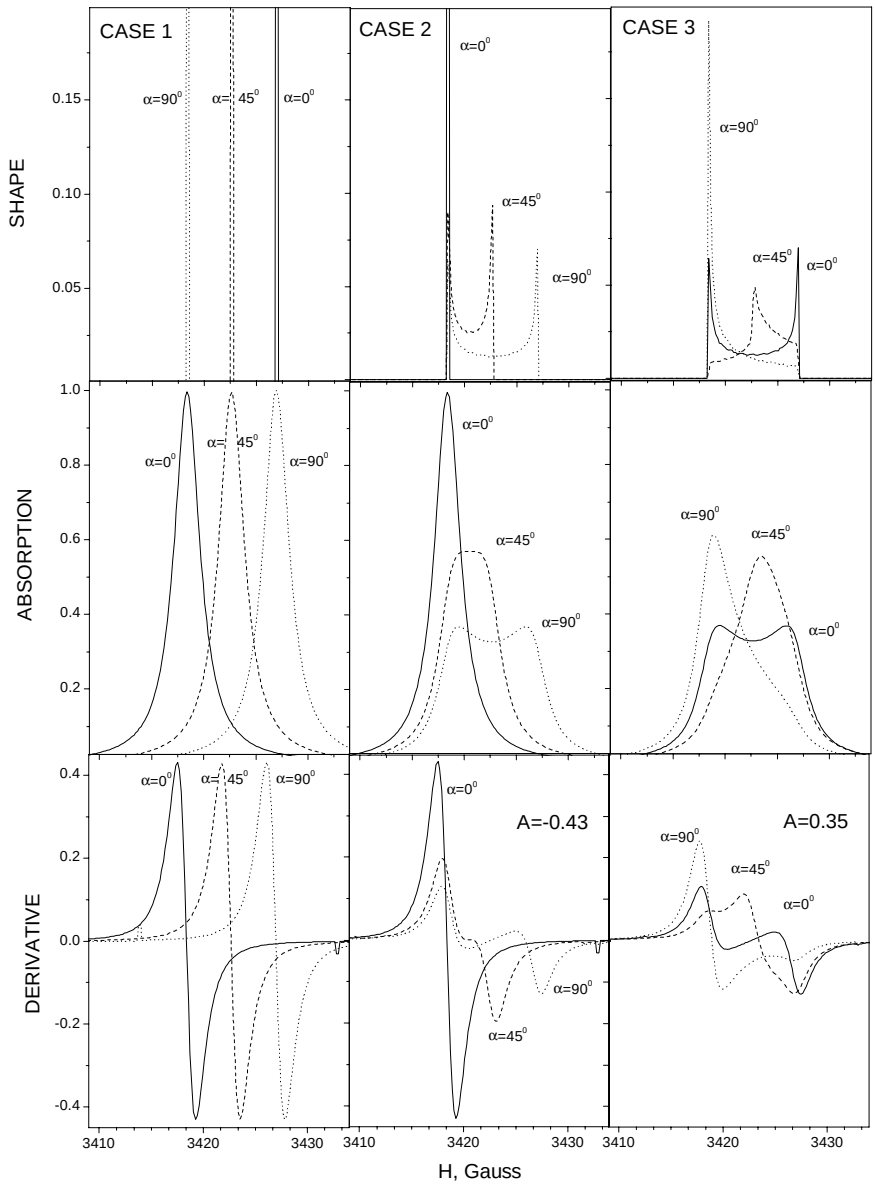

Fig. 12. Monte Carlo simulated shape function (g_x = 2.00255, g_y = 1.99754, gH = 6845.5), Lorentz convolute ($L = 2.25/[2.25 + (H - H_0)^2]$), and derivative spectrum of axial paramagnetic molecules on the cylindrical surface.

better comparison with the experiment the curves presented are of the same Lorentz width $\Gamma = 1.5\,\mathrm{G}$ as in the approximations in Sec. 4.1. Tensor components $g_x = 2.00255$ and $g_y = 1.99754$ are chosen corresponding to their values in hydroxyapatite monocrystals from a recent work of Vanhaelewyn et al. [26] and $gH = 6845.5$ for comparison with the measured spectra in Fig. 10.

Case 4 represents spectra that do not depend on orientation. This case is not depicted here.

To make a comparison with the above specific arrangements, two further cases will be considered.

Case 5

Molecules of axial symmetry with preferential orientation parallel to $\boldsymbol{K}$ ("fuzzy" case 1).

Case 6

Molecules of orthorhombic symmetry with preferential orientation parallel to $\boldsymbol{K}$.

Monte Carlo simulation has been made for case 5, where δ was chosen normal random in (8). Physically this means that radicals are oriented preferentially with their *y*-axes parallel to the surface normal and their misalignment can be reduced to a distribution of nanocrystalline *c*-axes. As was stated above, this case does not discriminate between the bulk and surface position.

From (8) it is convenient to express

$$\sin\delta = \sqrt{(g^2 - g_y^2)/(g_x^2 - g_y^2)}. \tag{11}$$

The value of $\delta g = 0.00001$ and the beginning value of the histogram were chosen such that the shape function approached a constant value at $g \to g_y$ (formula 11 gives zero if improperly applied). The shape function for molecules with *y*-axes distributed in the space angle $\Delta\delta = 30°$, Lorentz convolute with $\Gamma = 1.5\,\mathrm{G}$, and derivative spectra are presented in Fig. 13.

Monte Carlo simulation has also been done for case 6 with parameter values $g_y = 1.9975$, $g_z = 2.0019$, and $g_x = 2.0030$ for Gaussian distribution widths from 0° to 45°. In Fig. 13 simulated spectra are presented for the oriented molecules model, where α has the same values of 0°, 45°, and 90° as in the experimental spectra (Fig. 10), the normal distribution width $\Delta\beta$ is 22.5° or 32.5°, and convolution is made with a Lorentz function with $\Gamma = 1.5\,\mathrm{G}$, as was found optimal for the powder spectra. For $\sin\beta$ we used the expression (8) with $\beta = \delta$. This is a simplification resulting in a distortion of the shape function in the low field part of the spectrum that is not very large if g_x and g_z have close values and if the distribution width $\Delta\beta$ is not large.

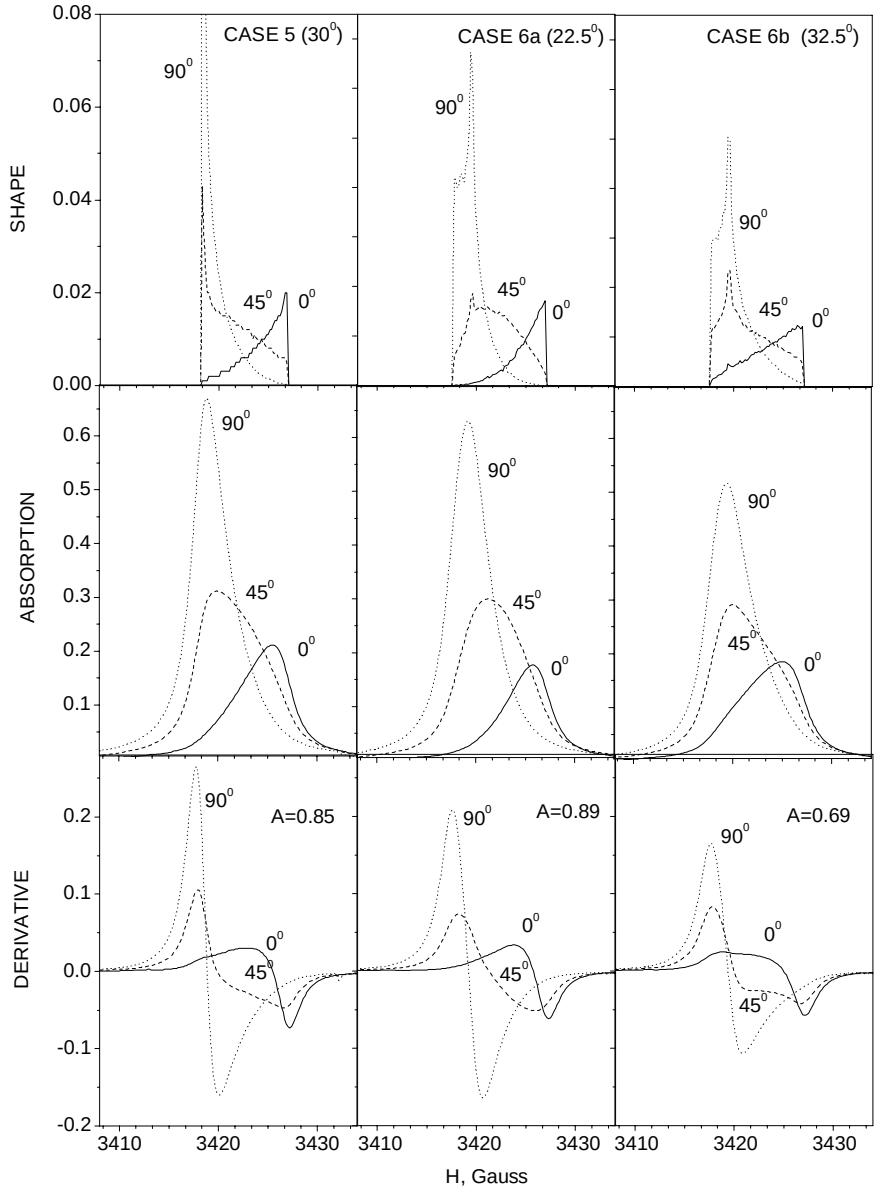

Fig. 13. Monte Carlo simulated shape function, Lorentz convolute, and derivative spectra for axial (case 5, column 1) and orthorhombic paramagnetic molecules (case 6a, column 2; case 6b, column 3).

5. DISCUSSION

When comparing the experimental spectra of the enamel fragment (Fig. 10) with the theoretical ones for the cylindrical surface (Fig. 12) one can see that

even a qualitative agreement is lacking. Obviously molecules on the surface are not oriented, having *y*-axes perpendicular to the cylindrical surface, neither are molecules in the bulk, with their axes randomly aligned in the plane perpendicular to ***C***. The shift of the measured band with α is opposite to case 2, but corresponds to case 1. Accordance with case 3 is better in the sense that the spectral order of bands is not reversed. However, the model shows persistence of the band at any angle α for g_x (at $H_x = 3417$ G) and an anisotropy parameter value much smaller than the experimental value ($A = 0.807$). If one allows for some misalignment of molecules on the surface, the agreement should be even worse. The same arguments apply also for molecules having orthorhombic symmetry if the anisotropy in the zx plane is small.

Bulk model with some misalignment of axes can be neatly fitted to the experiment. Both the first derivative spectral curves (take note of the 45° curve) and *A* value in Fig. 10 are intermediate between the orthorhombic models for the normal random distribution of angles in case 6 with $\Delta\beta = 22.5°$ (6a) and $\Delta\beta = 32.5°$ (6b) in Fig. 13. The axial model (case 5) with $\Delta\beta = 30°$ as well responds qualitatively to the experimental spectra. Some differences (e.g. areas under the absorption curves for different orientations) can be accounted for deviations from the normal distribution. However, the same picture is expected in the case of radicals situated on the surface with the *x*- and *z*-axes randomly oriented in the xz plane. In particular, a model with the *x*-axis perpendicular to the surface [4] is consistent with the above considerations. Therefore, there remains the possibility that molecules are on the surface with axes approximately along ***K*** ("fuzzy" case 1). This case cannot be distinguished from bulk arrangement solely on the EPR contour analysis. In [27] we present data supporting the presence of two kinds of radicals having different dose saturation characteristics. Other arguments for more than one kind of CO_2^- radicals in tooth enamel can be found in the literature [18,26].

It should be noted that in the first attempt to simulate EPR spectra of irradiated tooth enamel with misaligned crystallites [28] the authors used a combination of 12 Legendre polynomials. Their results, presented in the cited paper [28], were analysed only for making distinction between caries-sensitive and caries-resistant teeth, and it is hard to decide how many polynomials are actually needed for simulation. It is clear that, besides anatomic peculiarities, spectra depend also on geometrical characteristics, and anisotropy is better expressed in small fragments with uniformly arranged nanocrystals.

Vanhaelewyn et al. [26] analysed the spectra of radicals in monocrystals of synthetic hydroxyapatite containing carbon impurities. They found that CO_2^- radicals possess axial, not orthorhombic, symmetry and that there are two types of axially symmetric molecules with different *g*-splittings and different relaxation behaviour. At room temperature the parallel component of the *g*-tensor has the same value as g_y in the present work, but the perpendicular component of the *g*-tensor has the average value of the g_x and g_z in the present work. Rapid rotation

of the molecule around the *y*-axis is given as the reason for higher symmetry in hydroxyapatite monocrystals [26].

In tooth enamel the preferential arrangement confines itself to the hexagonal axes of nanocrystals; their perpendicular axes are obviously directed in a random manner. Independence of the EPR spectra of the angle of rotation around the surface normal of the carefully oriented enamel fragment (see also [19]) cannot be used as an argument for the axial local symmetry. We have approximated enamel powder spectra with both, axial and orthorhombic models and given preference to the latter because it led to smaller residuals. Given three (or more) different positions of CO_2^- radicals, there remains the possibility that in some of them molecules are tumbling around the O–O-axis and the resulting spectrum is a sum of axial and orthorhombic constituents.

Changes in the spectral anisotropy of tooth enamel with temperature have been described earlier (see [18] and references therein) and related to the reorientation of crystallites in the organic matrix. Without disclaiming the presence of metamorphic modifications of enamel we want to stress that the alignment of CO_2^- radicals we see in spectra does not reduce to thermal reorientation of nanocrystals in enamel. It is hard to believe that partial restoration of the powder-like spectrum by repeated irradiation leads to chaotic arrangement of nanocrystals, or that charges are trapped preferentially in nanocrystals that retained orientation during annealing. There are potential alternative explanations for reversible effects in spectra. Irradiation creates radicals in positions (in the bulk and on the surface layer) where they are randomly oriented. If the temperature rises, they can either reorient (over some activation barrier) or even change position by jumping into positions of high local symmetry [16]. Reirradiation adds new radicals from precursors, initially oriented randomly again. It is also possible that charge release from randomly oriented radicals and retrapping at precursors in high symmetry positions is partially responsible for developing anisotropy if trapping is thermally activated.

It is well known that thermally activated destruction of paramagnetic centres of various kinds in tooth enamel is quite complicated and not described with a simple Arrhenius law (e.g. [29]). Paramagnetic entities grow and perish also in the enamel that has not been irradiated, solely as the result of thermal treatment [30]. There are radicals of different thermal stability [16]. We have earlier made isochronal annealing experiments up to 460 °C and found that the high temperature end of thermal destruction of the CO_2^- signal can be described by the asymptotic value of $E_D = 1.3$ eV. Here we demonstrated that the temperature interval from 150 to 270 °C can be characterized by $E_D = 0.39$ eV in a sample that has been previously thermally cycled for many times. At still higher temperatures pyrolysis begins that needs higher activation energy for CO_2 to escape. The EPR signal of CO_2^- radicals disappears at this stage.

ACKNOWLEDGEMENTS

Tooth enamel samples were irradiated by the courtesy of Albrecht Wieser and Ülo Vaher. The ERS 230 spectrometer was repeatedly reanimated by Jaan Past. Discussions with Mihkel Veiderma on apatite chemistry and the help of Urmas Nagel with the software are appreciated. The work was supported by the Estonian Science Foundation (research grant No. 3838).

REFERENCES

1. *Proceedings of the 9th International Conference on Luminescence and Electron-Spin Resonance Dating (LED99), Rome, Italy, 6–10 September 1999*. In *Radiat. Meas*., 2000, **32** (McKeever, S. W. S., ed.) and *Quat. Sci. Rev.*, 2001, **20** (Grün, R. and Wintle, A. G., guest eds.).
2. Callens, F. J., Verbeeck, R. M. H., Matthys, P. F. A., Martens, L. C. and Boesman, E. R. The contribution of CO_3^{3-} and CO_2^- to the ESR spectrum near $g = 2$ of powdered human tooth enamel. *Calcif. Tissue Int.*, 1987, **41**, 124–129.
3. Elliott, J. C. *Structure and Chemistry of the Apatites and Other Calcium Orthophosphates*. Elsevier, Amsterdam, 1994.
4. Kenner, G. H., Haskell, E. H., Hayes, R. B., Baig, A. and Higuchi, W. I. EPR properties of synthetic apatites, deorganified dentine, and enamel. *Calcif. Tissue Int.*, 1998, **62**, 443–446.
5. Callens, F., Moens, P. and Verbeeck, R. An EPR study of intact and powdered human tooth enamel dried at 400 °C. *Calcif. Tissue Int.*, 1995, **56**, 543–548.
6. Scott, D. B. The electron microscopy of enamel and dentin. *Ann. New York Acad. Sci*., 1955, **60**, 575–584.
7. Trautz, O. R. X-ray diffraction of biological and synthetic apatites. *Ann. New York Acad. Sci*., 1955, **60**, 696–712.
8. Stack, M. V. The chemical nature of the organic matrix of bone, dentin, and enamel. *Ann. New York Acad. Sci.*, 1955, **60**, 585–595.
9. Doi, Y., Koda, T., Adachi, M., Wakamatsu, N., Goto, T., Kamemizu, H., Moriwaki, Y. and Suwa, Y. Pyrolysis-gas chromatography of carbonate apatites used for sintering. *J. Biomed. Mater. Res*., 1995, **29**, 1451–1457.
10. von Kühl, G. and Nebergall, W. H. Hydrogenphosphat- und Carbonatapatite. *Z. Anorg. Allg. Chemie*, 1963, **324**, 313–320.
11. Geoffroy, M. and Tochon-Danguy, H. J. Long-lived radicals in irradiated apatites of biological interest: an e.s.r. study of apatite samples treated with $^{13}CO_2$. *Int. J. Radiat. Biol*., 1985, **48**, 621–633.
12. Moens, P., Callens, F., Matthys, P., Maes, F., Verbeeck, R. and Naessens, D. Adsorption of carbonate-derived molecules on the surface of carbonate-containing apatites. *J. Chem. Soc. Faraday Trans*., 1991, **87**, 3137–3141.
13. Suetsugu, Y., Hirota, K., Fujii, K. and Tanaka, N. Compositional distribution of hydroxyapatite surface and interface observed by electron spectroscopy. *J. Mater. Sci.*, 1996, **31**, 4541–4544.
14. Lunsford, J. F. and Jayne, J. P. Formation of CO_2^- radical ions when CO_2 is adsorbed on irradiated magnesium oxide. *J. Phys. Chem.*, 1965, **69**, 2182–2184.
15. Callens, F. J., Verbeeck, R. M. H., Naessens, D. E., Matthys, P. F. A. and Boesman, E. R. The effect of carbonate content and drying temperature on the ESR-spectrum near $g = 2$ of carbonated calciumapatites synthesized from aqueous media. *Calcif. Tissue Int.*, 1991, **48**, 249–259.
16. Liidja, G. EPR study of tooth enamel: temperature effects on CO_2^- radicals. *Phosphorus Res. Bull.*, 1999, **10**, 341–346.

17. Aoba, T., Doi, Y., Yagi, T., Okazaki, M., Takahashi, J. and Moriwaki, Y. Electron spin resonance study of sound and carious enamel. *Calcif. Tissue Int*., 1985, **34**, S88–S92.
18. Brik, A., Radchuk, V., Shcherbina, O., Matyash, M. and Gaver, O. Metamorphic modifications and EPR dosimetry in tooth enamel. *Appl. Radiat. Isot*., 1996, **47**, 1317–1319.
19. Rossi, A. M. and Poupeau, G. Radiation damage in bioapatites: the ESR spectrum of irradiated dental enamel revisited. *Nucl. Tracks Radiat. Meas.*, 1990, **17**, 537–545.
20. Moens, P., De Volder, P., Hoogewijs, R., Callens, F. and Verbeeck, R. Maximum-likelihood common-factor analysis as a powerful tool in decomposing multicomponent EPR powder spectra. *J. Magn. Res*., 1993, **A101**, 1–15.
21. Chumak, V. et al. The first international intercomparison of EPR dosimetry with teeth: first results. *Appl. Radiat. Isot*., 1996, **47**, 1281–1291.
22. Jonas, M. and Marseglia, E. The case for the use of integrated spectrum disconsolation in ESR dating – a numerically generated example. *Radiat. Meas.*, 1997, **27**, 359–363.
23. Grün, R. Methods of dose determination using ESR spectra of tooth enamel. *Radiat. Meas.*, 2000, **32**, 767–772.
24. Callens, F., Verbeeck, R., Martens, L., Matthys, P. and Boesman, E. Electron spin resonance absorption of centres with an orthorhombic *g*-tensor in polycrystalline substances. *Phys. stat. sol. (a)*, 1986, **94**, 267–274.
25. Kneubühl, F. K. Line shapes of electron paramagnetic resonance signals produced by powders, glasses, and viscous liquids. *J. Chem. Phys.*, 1960, **33**, 1074–1078.
26. Vanhaelewyn, G. C. A. M., Morent, R. A., Callens, F. J. and Matthys, P. F. A. E. X- and Q-band electron paramagnetic resonance of CO_2^- in hydroxyapatite single crystals. *Radiat. Res*., 2000, **154**, 467–472.
27. Liidja, G. and Wieser, A. EPR of tooth enamel at high gamma ray doses (submitted to *Radiat. Prot. Dosim.*).
28. Cevc, G., Cevc, P., Schara, M. and Skalerič, U. The caries resistance of human teeth is determined by the spatial arrangement of hydroxyapatite microcrystals in the enamel. *Nature*, 1980, **286**, 425–426.
29. Hennig, G. J. and Grün, R. ESR dating in Quaternary geology. *Quat. Sci. Rev*., 1983, **2**, 157–238.
30. Fattibene, P., Aragno, D., Onori, S. and Presselo, M. C. Thermal induced EPR signals in tooth enamel. *Radiat. Meas.*, 2000, **32**, 793–798.

ORIENTEERITUD NANOKRISTALLIDEGA HAMBAEMAILI ELEKTRONIDE PARAMAGNETRESONANTSI SPEKTRID

Georg LIIDJA

Gamma-kiiritatud hambaemaili fragmendi elektronide paramagnetresonantsi spekter omandab anisotroopse iseloomu pärast kuumutamist temperatuuril üle 150°C. Pärast teistkordset kiiritamist on spektri anisotroopia vähenenud (spekter läheneb pulbri tüüpi spektrile), kuid teistkordne termiline töötlemine taastab anisotroopia. Spektri anisotroopia kirjeldab hüdroksüapatiidi nanokristallide kogumit, milles heksagonaalse sümmeetriaga kristallide *c*-teljed on valdavalt risti hamba välispinnaga. Hea kooskõla mõõdetud spektrite sõltuvusega fragmendi orientatsioonist magnetvälja suhtes annab Monte Carlo tüüpi spektrisimulatsioon, mis lähtub paramagnetiliste CO_2^- molekulide asetusest kristallivõres, nii et ortorombilise (või aksiaalse) sümmeetriaga molekulide *y*-teljed moodustavad normaalse jaotuse ruuminurgas 27° (±5°) ümber pinnanormaali suuna. Alternatiivsed mudelid, mis on tuletatud CO_2^- molekulide spetsiifiliste pindasetuste jaoks, ei ole eksperimendiga kooskõlas.